Diagnosis of Three-Dimensional Water Vapor Using a GPS Network

ALEXANDER E. MACDONALD AND YUANFU XIE*

Forecast Systems Laboratory, NOAA/OAR, Boulder, Colorado

RANDOLPH H. WARE

GPS Science and Technology Program, University Corporation for Atmospheric Research, Boulder, Colorado

(Manuscript received 26 June 2000, in final form 5 January 2001)

ABSTRACT

In recent years techniques have been developed to obtain integrated water vapor along slant paths between ground-based Global Positioning System (GPS) receivers and the GPS satellites. Results are presented of an observing system simulation (OSS) to determine whether three-dimensional water vapor fields could be recovered from a high-resolution network (e.g., with 40-km spacing) of GPS receivers, in combination with surface moisture observations and a limited number of moisture soundings. The paper describes a three-dimensional variational analysis (3DVAR) that recovers the moisture field from the slant integrated water vapor and other observations. Comparisons between ''nature'' moisture fields taken from mesoscale models and fields recovered using 3DVAR are presented. It is concluded that a high-resolution network of GPS receivers may allow diagnosis of three-dimensional water vapor, with applications for both positioning and mesoscale weather prediction.

1. Introduction

It has been shown that vertically integrated water vapor can be determined from the constellation of GPS satellites by isolating the effects of signal delay due to atmospheric water vapor (Bevis et al. 1992). Recently, techniques have been developed to determine the amount of phase delay between surface receivers and each of a number of the satellites that are in view (Alber et al. 2000; Braun et al. 2001, hereafter BRW). With a good estimate of the three-dimensional mass of the atmosphere, the amount of water vapor along the slant path can be estimated from the phase delay. These techniques, referred to as ''slant'' water vapor measurements, can significantly increase the information available about water vapor. Experiments presented here address whether three-dimensional variational analysis can recover a three-dimensional water vapor field using many integrated slant water vapor measurements from each of numerous stations in a horizontal grid. The technique requires an accurate lower boundary condition, such as the surface moisture measured by the network and other surface stations. The addition of a few moisture soundings per hour improve the convergence and accuracy of the three-dimensional field.

Water vapor is very important to short-range weather prediction (Emanuel et al. 1995). Precipitation and severe weather are closely related to the three-dimensional distribution of water vapor, yet skill in these predictions has been slow to improve. This is mainly due to the high spatial variability of water substance, as can be seen daily in satellite and radar images. As computer speeds increase, the ability of mescoscale prediction models to use high-resolution information will increase. Thus there is reason to hope that much better observations of three-dimensional water vapor would result in significant improvements in weather prediction.

In recent years there has been extensive study of the role that GPS water vapor measurements could play in weather prediction. The assimilation of precipitable water into a mesoscale model was first shown by Kuo et al. (1993). Later studies addressed variational assimilation of precipitable water into nonhydrostatic models (Kuo et al. 1996; Guo et al. 2000). These concepts are being tested with data from low-resolution networks (Wolfe and Gutman 2000; Ware et al. 2000). The concept of this study differs from earlier studies by assuming that the large amount of additional information obtained by use of slant water vapor delays could be used in a mesoscale (e.g., 40-km) resolution network to directly diagnose three-dimensional water vapor structure. The variation of water vapor in the vertical direction, made possible by the use of the slant measurements, is

* Additional affliation: Cooperative Institute for Research in the Atmosphere, Colorado State University, Boulder, Colorado.

Corresponding author address: A. E. MacDonald, NOAA Forecast Systems Laboratory, R/FS, 325 Broadway, Boulder, CO 80305.
E-mail: macdonald@fsl.noaa.gov

Unauthenticated | Downloaded 04/01/23 09:52 AM UTC

very valuable in both numerical and human weather prediction.

The main thrust here is to present the results of a test that addresses how well a high-resolution network of GPS receivers would recover three-dimensional water vapor fields. The test consists of the creation of a ''nature'' field of water vapor and the use of hypothetical observations from the nature atmosphere, including estimates of observational errors. The hypothetical observations of surface moisture and many measurements of slant water vapor are used as input to the three-dimensional variational (3DVAR) analysis. The resulting field is then compared with the nature atmosphere. We refer to this as an observing system simulation (OSS). A further step in determining the role of an observing system on a predictive model is generally referred to as an observing system simulation experiment or OSSE. We show the results of two observing system simulations, but do not address prediction differences (OSSEs), which may be the subject of future studies.

In the next section, we discuss the measurement of slant water vapor using GPS techniques. In section 3 we hypothesize a network design that could be used to recover three-dimensional water vapor fields and describe an OSS to test the concept. In section 4 we present the 3DVAR that is used in the OSS, and in section 5 we present the simulation results.

2. GPS sensing of slant water vapor

There are several approaches to GPS sensing of atmospheric water vapor from the ground. Bevis et al. (1992) used standard space geodetic techniques (e.g., Segall and Davis 1997) to estimate the 2–3-m zenith phase delay induced in GPS signals by the neutral atmosphere. Residual signal delays to each satellite can be mapped as a function of the cosecant of the satellite elevation angle (Niell 1996; Rocken et al. 2001), based on the assumption that the atmosphere is azimuthally homogeneous. This gives an average zenith delay from which the hydrostatic, or ''dry'' component estimated from surface pressure is subtracted. Precipitable water vapor (PW) is calculated as the product of the zenith delay and a conversion factor (Bevis et al. 1994). The accuracy of GPS-sensed PW by this method is better than 2 mm (e.g., Rocken et al. 1993; Fang et al. 1998).

The assumption of azimuthal symmetry (Davis et al. 1993; Elosegui et al. 1999) limits the accuracy and spatial resolution of GPS-sensed PW. Higher spatial resolution can be obtained by solving for the integrated water vapor or slant water (SW) along each GPS ray path. The SW is obtained by solving for the total slant delay along each ray path, and then subtracting the dry component of the slant delay. The dry slant delay can be estimated from three-dimensional numerical weather models (Chen and Herring 1997) by integrating dry air mass along the path. Alternatively, total slant delays could be assimilated directly into meteorological models, allowing the model to partition the wet and dry components.

The formula for calculating signal delay between a surface station and a satellite on a slant path is given by Kaplan (1996):

$$\text{slant delay} = \overbrace{C_1 \int_{\text{surface}}^{\text{satellite}} \rho_a \, ds}^{\text{dry delay}} + \overbrace{C_2 \int_{\text{surface}}^{\text{satellite}} \rho_{\text{wv}} \, ds + C_3 \int_{\text{surface}}^{\text{satellite}} \frac{\rho_{\text{wv}}}{T} \, ds}^{\text{moist delay}},$$

where ds is along slant path

$$\rho_a = \text{atmospheric density},$$

$$\rho_{\text{wv}} = \text{water vapor density},$$

$$T = \text{atmospheric temperature},$$

and C_1, C_2, and C_3 are constants.

In this formula it is assumed that the ionospheric delay has been removed. It can be seen that the ''dry delay'' is due to the presence of atmospheric mass between the receiver and the satellite, and the moist delay arises from two effects: the first term is the effect of water vapor mass, and the second is induced by the dipole moment of the water molecule.

3. Design

a. Hypothetical network design

Our goal is to recover high-resolution (mesobeta) three-dimensional water vapor from a network of ground-based GPS receivers. To resolve this scale, the network must have a spacing comparable to the desired resolution. A grid of stations over the United States (excluding Alaska) at 40-km spacing would include about 5000 installations, while a grid of 60-km spacing would require a little more than 2000 installations. It is clear that there is a trade-off to be made between the number of the stations in the surface network and the cost of the system.

The operational concept includes a typical ground installation with a dual-frequency GPS receiver and an automated surface weather station measuring winds, temperature, and humidity. The number of GPS satellites in view from the surface would average about eight. We assume that with suitable time integration and averaging, there is one observed slant range between each station and each satellite every 5 min. Thus, for each station, there are approximately 100 observations of slant range moisture per hour. The observations are distributed around the hemisphere, with the exception of the northern quadrant, as discussed in Rocken et al.

Unauthenticated | Downloaded 04/01/23 09:52 AM UTC

(1997). The geometry of the system allows more observations in the 45° closest to the zenith than in the 45° above the horizon, but there are typically several satellites rising or setting during the 1-h period. We refer to the ''splay'' of slant ranges as the dataset taken during an observing period, which in our case is taken to be 1 h. In addition to the integrated slant water vapor measurements, there are two other types of observations used in the 3DVAR. The inclusion of an accurate moisture sensor at each station allows the integrals of slant water vapor to start from the surface with a known value, which is a very valuable constraint in the variational analysis. In addition, a low density of water vapor soundings (e.g., from microwave radiometers, Solheim et al. 1998) is needed to constrain the analysis.

An important characteristic of the network would be to resolve moisture in the lowest layers of the atmosphere. It is an observational fact that moisture is generally greatest near the surface, and typically decreases upward with a scale height of about 2500 m. The boundary layer, which is normally 1000–3000-m deep, is very important in weather prediction. For example, showers and thunderstorms are usually driven by moisture-laden plumes originating in the boundary layer (Emanuel et al. 1995). The use of the low angles allows resolution of the moisture to within approximately 250 m above the surface, with resolution of 500 m above. The density of stations and the lowest usable slant angle both determine the minimum altitude that the GPS network would be sampling. At lower slant ranges, say, less than 6°, the measurement of slant range water vapor has some associated difficulties. Most important are blockage due to the terrain horizon, reduced signal strength, and multipath effects in which the signal is reflected from surface objects. Despite these difficulties, there is evidence that usable slant range water vapor can be obtained down to the horizon (Ware et al. 1997). A recent test that measured GPS bending angles from a surface receiver (Sokolovskiy et al. 2001; Lowry et al. 2001) showed that the GPS-measured refractivity agreed well with collocated radiosondes all the way to the surface.

b. Observing system simulation

An OSS begins with the creation of a dataset with the goal of emulating nature. Ideally, if there were an experiment where moisture soundings were taken at 10-km spacing over a large domain (e.g., 1000 or more kilometers on a side), this dataset could be used to represent nature for a simulation. Unfortunately, such a dataset does not exist. Since we do not have such realistic field measurements, a technique must be used to create a nature field that is reasonable. By reasonable, we mean that the characteristics of the field, such as its power spectrum, spatial distribution, including typical gradients, etc., must be like those found in the real atmosphere. We assumed in this experiment that state-of-the-art high-resolution mesoscale models could create water vapor fields that are similar to those found in the real atmosphere.

In the OSS described here, we used two mesoscale models to create nature atmospheres over an approximately square domain with sides of 1460 km centered in the west-central United States. The domain was chosen to include the lower, flatter topography of the Great Plains on the east side and the complex terrain of the Rocky Mountains. This also meant a gradient of moisture, with high specific humidities in the eastern area, and in the west the low humidities characteristic of the mountains. The two models used were the quasi-nonhydrostatic (QNH) model of MacDonald et al. (2000) and the Pennsylvania State University–National Center for Atmospheric Research fifth generation Mesoscale Model (MM5; Dudhia 1993). Both models were run at 10-km resolution for 36 h, with the three-dimensional water vapor at the end of the period taken as the nature dataset. Each model has a full microphysics package, with at least five water forms (vapor, rain, snow, cloud water, and cloud ice) and the associated phase changes. Both models develop complex moisture fields in three dimensions, with high gradients in both the horizontal and vertical directions. As has been seen in aircraft measurements of water vapor fields (e.g., Palmen and Newton 1969), the spatial variance on mesobeta scales is quite large. The reasons for this variability are well known: they include nonlinear scale collapse, and the fact that when high gradients develop in water vapor fields, generally only diffusive processes operate to even them out. This characteristic is in contrast to the dynamic fields in which a high gradient (e.g., of temperature) causes strong adjustment processes that operate to decrease spatial variability. Another process that operates to generate complex moisture fields is the combination of phase change, such as condensation, and gravity. A dry lower atmosphere can be penetrated by a rain shaft, with the resulting evaporation generating strong moisture gradients. In the two cases used for nature runs, all of these processes operated to create complex and realistic-looking three-dimensional moisture fields.

The QNH model was initialized in April 1999, while the MM5 run was from a late January 1999 case. Thus the results are representative of a moist springtime moisture field and a drier, colder winter moisture field. Both models showed the results of small-scale precipitation processes, which had generated small areas of enhanced water vapor, an important test for the hypothetical system. As will be shown in section 5, the technique was able to recover this structure, albeit slightly smoothed.

The next step in the OSS is to use the nature field to generate pseudo-observations of the slant water vapor, the surface moisture fields, and the soundings. These pseudo-observations from the network are used as input to the variational analysis that attempts to approximate the nature field. A number of precautions were taken to make the data realistic. The pseudo-observations of wa-

Unauthenticated | Downloaded 04/01/23 09:52 AM UTC

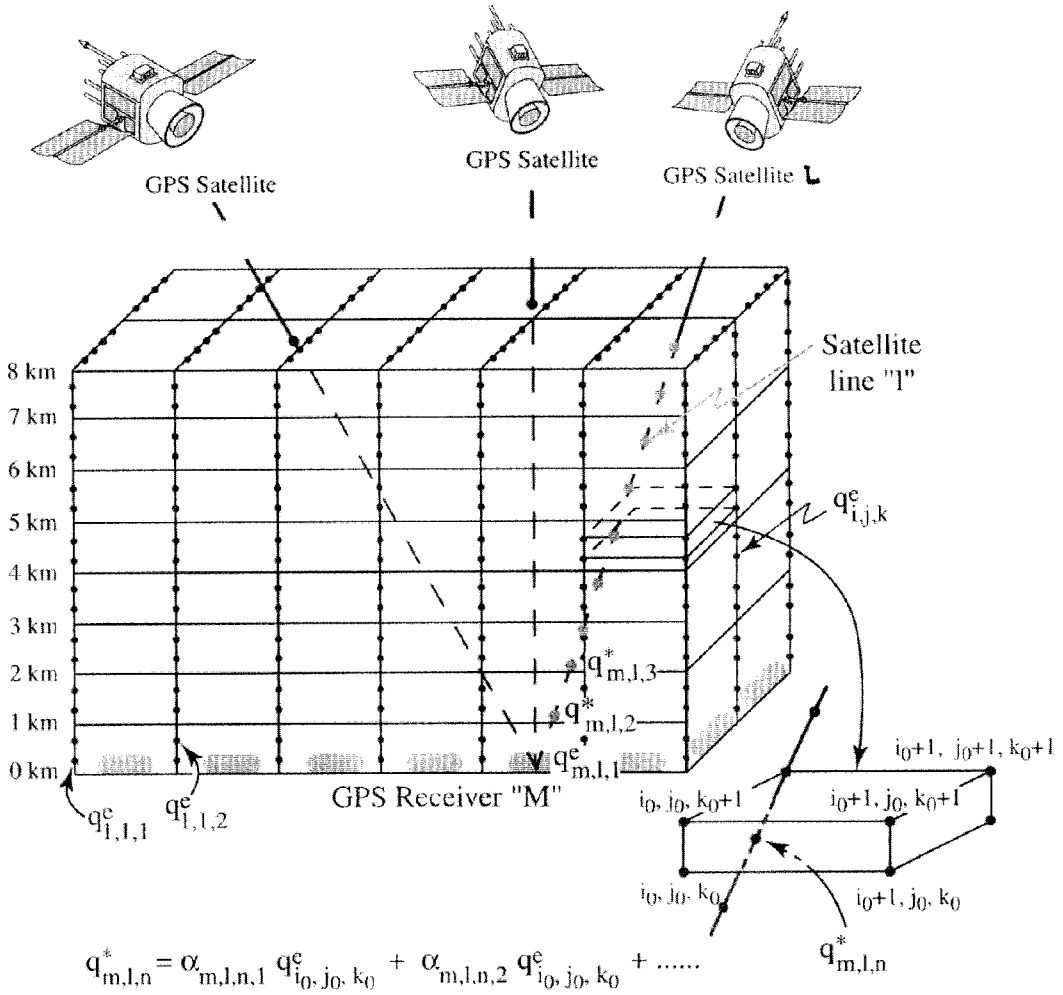

FIG. 1. A schematic of the grid used for the 3DVAR analysis. Surface stations are represented by grey ovals at 0 km. The line between surface station M and satellite L is referred to as line *m, l.* Control grid points are identified by $q^e_{i,j,k}$. The forward model is the estimate of the line integral $q^*_{m,l}$ from the control grid q^e.

ter vapor were randomly perturbed by a 5% error function, which was based on estimates of random error by BRW. For lower angles, below 6°, the error was increased to 7%. Also, those slant paths that penetrated the lateral boundary were perturbed with 7% errors. Note that ground-based GPS stations do not measure integrated water vapor, but rather integrated delay, which includes effects due to atmospheric mass between the receiver and the satellite, and ionospheric delay, as discussed in section 2. The chosen error bounds include errors due to these effects, and thus makes it reasonable to analyze the system in terms of water vapor delays. It was not assumed that the stations could be located precisely on a grid; a busy highway would not be a good place to site a station. The station locations were perturbed in a ring around the nominal station grid points, with an average ''location change radius'' of 5 km. The surface moisture readings were assumed to have random errors of 5%, and the vertical soundings were given average moisture errors of 8% based on statistical comparison with radiosondes (Güeldner and Spänkuch 2001).

In order to collect enough pseudo-observations, there is an assumption of stationarity for the water vapor field. All observations for an hour are treated in the variational analysis as if they represent a single field. This implies that for the very small scale (e.g., less than 20 km), rapid changes in the moisture field will not be resolved. To make the OSS realistic, we used the actual ephemeris data to locate the satellites every 5 min. The significant motion of the satellites causes each measurement to be made in a different direction, making the measurements somewhat independent. Furthermore, the model moisture data were allowed to change through the hour by use of the actual 5 min data from the model run.

The OSS is properly defined if realistic errors for the observations are included. In particular, if a technique for recovery of slant water vapor is tested against an-

Unauthenticated | Downloaded 04/01/23 09:52 AM UTC

other observing system and the average error of the water vapor is determined, then no other information is necessary for the simulation. Slant water vapor measurements using GPS have been validated by comparison with microwave radiometers to determine the errors used in this simulation (BRW). This does not imply that this approach would be used in an operational system. It is likely that additional information could be gleaned by using total delay in an operational variational analysis, which would provide temperature as well as moisture information. We have isolated the moisture in this simulation to simplify the exposition.

There are two techniques possible for recovery of water vapor. First, the 3DVAR could use total delay, and be formulated to recover both temperature and water vapor. This approach is currently being investigated by the authors. A second technique is to take the mass field as a given, with an assumed error. In the second technique, a future operational system for water vapor would use the latest and best analysis of the mass field available to calculate the dry delay. For example, the Rapid Update Cycle (RUC) model now has hourly analysis (Smith et al. 2001) of the mass field and could be used to isolate the dry delay due to mass from the unknown wet delay. This procedure would work well except in those cases where the delays are strongly correlated and not accommodated in the model analysis. For example, an area of heavy rain showers falling into a dry lower layer can result in cooling and moistening of the layer. Both the cooling and moistening result in an increased signal delay between the satellite and the receiver. Thus, an operational analysis system would be best if it used measurements such as hourly surface pressure changes, and estimates of evaporative cooling to refine the mass field before use in the moisture-based 3DVAR analysis. The separation of dry delay from moist delay constitutes a significant assumption in this analysis and will need to be further tested, both theoretically and experimentally.

With the pseudo-observations from the nature atmosphere, a 3DVAR is used to determine the three-dimensional distribution of water vapor. Here, we use a simple version of 3DVAR in which it is assumed that the errors in the pseudo-observations of slant range water vapor are randomly distributed and uncorrelated with one another. We do not use a model background. In a more realistic future analysis, background errors would also need to be considered. Theoretically, the assumption of random errors is not too bad (Kaplan 1996), and should not invalidate the main conclusions of the study.

Figure 1 is a schematic of the network and grid used for the 3DVAR analysis. The small ovals on the bottom are the symbols for the GPS receivers and associated surface humidity sensors. The regularly spaced dots on the grids are the locations of the control points. At each control point, the 3DVAR has a control variable, the estimated water vapor (specific humidity), that will be iterated through a series of estimates toward the best estimate field. Each GPS receiver has an associated splay of pseudo-observations of integrated slant water vapor, and an estimated slant water vapor from the control grid (e.g., the forward model) is obtained by interpolating and using a Riemann sum. The number of con-

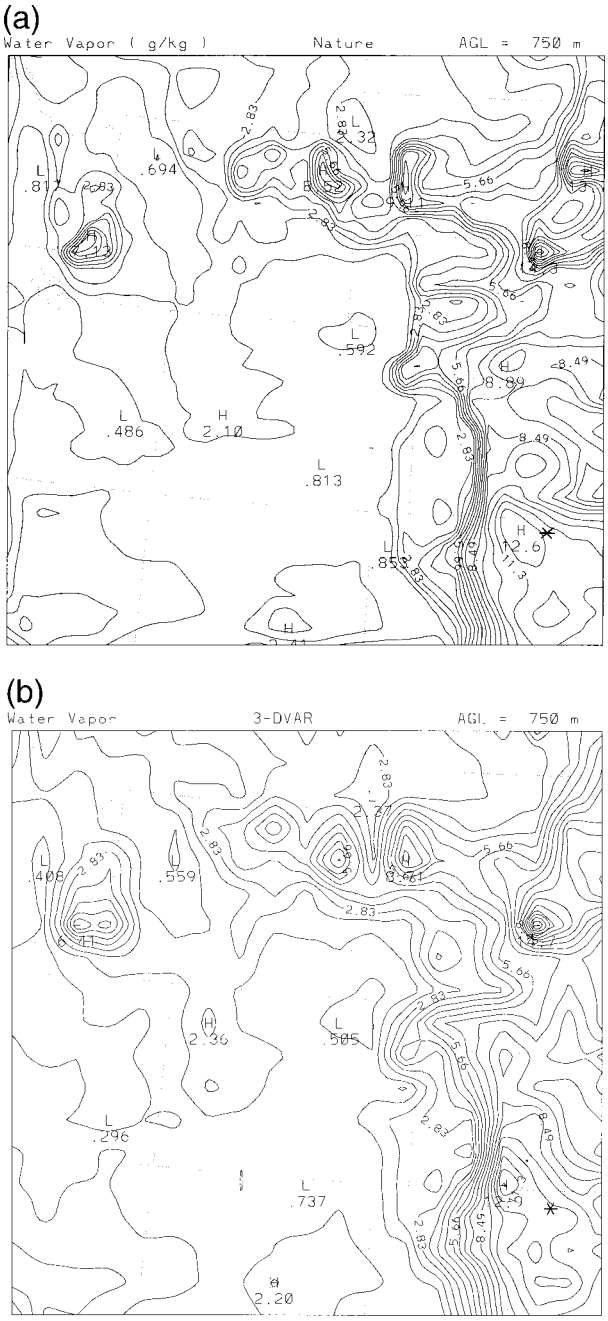

FIG. 2. Horizontal plots of specific humidity in g kg^{-1} for (a) the nature run, and (b) the 3DVAR analysis at the 750-m level. The nature run is from an Apr run of the QNH model. Notice the ''dryline'' along the west side of the Texas Panhandle into Kansas. It is clearly evident in the 3DVAR, albeit somewhat smoother. The location of the skew-*T* comparison in Fig. 5 is marked by an asterisk in the lower right corner.

Unauthenticated | Downloaded 04/01/23 09:52 AM UTC

trol points in the grid must be exceeded by the number of observations in order for the 3DVAR problem to be well determined. In the cases presented here, a 40-km resolution network and control grid can be well determined if there are approximately 100 observations per station, as discussed in section 3a.

The 3DVAR control grid is formulated with 40-km resolution in the horizontal and 500 m in the vertical. Our first attempt at an OSS 3DVAR used 40-km model data. This had very rapid convergence and excellent correspondence to the nature run. However, we thought that it was unrealistic to use such a low-resolution nature run, because it would not perturb that analysis with smaller scale variability. When we tried to run the 3DVAR analysis using 10-km model data, it was much more difficult to obtain convergence. As discussed in section 4, we needed to use a multigrid technique to get convergence when the high-resolution model data were used. We think that the 16-fold increase in model data points, which enters the problem through the pseudo-observations, realistically accommodates the variability that will be seen in the real atmosphere. It should be noted that although it was more difficult to obtain convergence with the high-resolution data, the improved techniques resulted in excellent convergence, as will be shown in section 6. However, it is possible that mesogamma-scale variability, associated with clouds, may cause difficulties. These could be tested with a higher resolution nature model.

4. Variational formulation

In this section we present the mathematical formulation of the 3DVAR problem. The simulation starts with a set of observations of the GPS slant integrated water vapor and a first guess of the water vapor field. In general, if an integral of precipitable water along a slant path is calculated numerically from the first-guess grid, it will differ significantly from the actual observation for the slant water vapor. We call the grid of estimated water vapor specific humidity the control grid. The idea is to iterate the estimated grid values to minimize the difference between the actual observations and the estimates from the control grid. We start by computing an estimate for slant water vapor from the control grid.

a. GPS line integral

We compute an estimated integrated water vapor using the grid values along each GPS line, $c_{m,l}$, which starts from a ground station G^m located at (x^m, y^m) and points to a satellite S^l. Denote this quantity as $Q^e(x^m, y^m, l)$. That is,

$$Q^e(x^m, y^m, l) = \int_{c_{m,l}} q\, ds,$$

which can be approximated using the values of $q_{i,j,k}$, the specific humidity for a grid box. First the integral can be approximated by

$$\int_{c_{m,l}} q\, ds = \sum_{n=1}^{N} q(c_{m,l,n})\Delta s,$$

where $c_{m,l,n}$ is a sequence of equally spaced points on the curve $c_{m,l}$ and Δs is the length between two adjacent points. Therefore, we have the following approximation:

$$\begin{aligned} Q^e(x^m, y^m, l) &\simeq \tilde{Q}^e(x^m, y^m, l) \\ &= \Delta s \sum_{n=1}^{N} (\alpha^{m,l,n}_{1,1,1} q_{i_0(n),j_0(n),k_0(n)} + \alpha^{m,l,n}_{2,1,1} q_{i_0(n)+1,j_0(n),k_0(n)} + \alpha^{m,l,n}_{1,2,1} q_{i_0(n),j_0(n)+1,k_0(n)} + \alpha^{m,l,n}_{2,2,1} q_{i_0(n)+1,j_0(n)+1,k_0(n)} \\ &\quad + \alpha^{m,l,n}_{1,1,2} q_{i_0(n),j_0(n),k_0(n)+1} + \alpha^{m,l,n}_{2,1,2} q_{i_0(n)+1,j_0(n),k_0(n)+1} + \alpha^{m,l,n}_{1,2,2} q_{i_0(n),j_0(n)+1,k_0(n)+1} + \alpha^{m,l,n}_{2,2,2} q_{i_0(n)+1,j_0(n)+1,k_0(n)+1}), \end{aligned}$$

where the αs are the bilinear interpolation coefficients and $[i_0(n), j_0(n), k_0(n)]$ are the lowest indices of a grid cell containing the point $c_{m,l,n}$.

b. The cost function and its gradient

The cost function is used to represent the difference between the slant water vapor observations and the approximations of slant water vapor calculated from the control grid. The cost function is defined as

$$f = \frac{1}{2} \sum_{m=1}^{M} \sum_{l=1}^{L_m} [\tilde{Q}^e(x^m, y^m, l) - Q^o(x^m, y^m, l)]^2.$$

This typical optimization problem can be solved by numerical optimization algorithms. The technique we have chosen requires the gradient of the cost function.

c. Optimization technique

To minimize the cost function, a fairly large-scale minimization problem, the limited memory BFGS (L-BFGS) method (Liu and Nocedal 1989), is used. The BFGS method is a quasi-Newton method which has faster convergence rate than the steepest descent algorithms. Suppose at the nth iteration, we have an approximation $\mathbf{G}^n$ of the solution $\mathbf{G}^*$, where $\mathbf{G}$ is a vector with elements of $q_{i,j,k}$, and an approximation of the Hes-

Unauthenticated | Downloaded 04/01/23 09:52 AM UTC

sian of f at $\mathbf{G}^n$, $\mathbf{B}^n \simeq \nabla^2 f$. The BFGS method obtains new approximations by

$$\mathbf{G}^{n+1} = \mathbf{G}^n - (\mathbf{B}^n)^{-1}\nabla f(\mathbf{G}^n), \quad \text{and}$$

$$\mathbf{B}^{n+1} = \mathbf{B}^n - \frac{\mathbf{B}^n \mathbf{s}_n \mathbf{s}_n^{\mathrm{T}} \mathbf{B}^{n\mathrm{T}}}{\mathbf{s}_n^{\mathrm{T}} \mathbf{B}^n \mathbf{s}_n} + \frac{\mathbf{Y}_n \mathbf{Y}_n^{\mathrm{T}}}{\mathbf{s}_n^{\mathrm{T}} \mathbf{Y}_n},$$

where

$$\mathbf{s}_n = \mathbf{G}^{n+1} - \mathbf{G}^n, \quad \text{and} \quad \mathbf{Y}_n = \nabla f(\mathbf{G}^{n+1}) - \nabla f(\mathbf{G}^n).$$

To further restrict the solution, we solve this minimization problem with a simple bound, $q_{i,j,k} \geq 0$. In the numerical tests, we use the L-BFGSB algorithm developed by Byrd et al. (1995).

The 3DVAR analysis is initialized with a first guess. This was constructed by taking the surface values of the water vapor specific humidity and assuming an exponential drop-off with altitude, with an e-fold radius in the vertical of 2500 m. With an initial guess, the L-BFGSB algorithm starts iterating until a certain termination criterion is met.

d. Multigrid technique

We were able to solve the 3DVAR problem with the above formulation and algorithm. However, to counter a very noisy moisture field, we had to smooth the field in order to see the large-scale features. A very slow reduction of the cost function after the initial 10–20 iterations convinced us that the optimization algorithm spent most of the iterations converging the small-scale features and improved the long waves very little. This suggested that a multigrid technique could be helpful in improving the convergence of the longer waves. Thus, we combined the multigrid technique and the L-BFGSB algorithm in our numerical experiments. The multigrid technique is implemented with two multigrid levels, 40- and 80-km grids, over the same domain. We ran 10 iterations of the L-BFGSB algorithm to reduce the cost function over the 40-km grid and then projected the solution of the 40-km grid to the 80-km grid. On the 80-km grid, we ran 20 iterations of the L-BFGSB algorithm to reduce the new cost function over the 80-km grid and obtained an approximate solution. Then we interpolated the solution to the 40-km grid and ran 10 iterations of L-BFGSB algorithm again. This procedure, one multigrid cycle, can be repeated. We repeated this cycle 10 times. As a result, the solutions showed good convergence in the long waves without any smoothing. The multigrid and the uniqueness of the solution are discussed in MacDonald and Xie (2000).

5. Results

We present two types of results. First, we present depictions of the nature fields, and the fields recovered from the variational analysis for comparison. Second, we show several quantitative comparisons of the improvement in the analysis that could result from the proposed network.

a. Depiction of the nature and 3DVAR fields

Several depictions of fields were obtained from the 3DVAR analysis for comparison with the nature fields. For the horizontal depictions, we display the specific humidity. In this OSS, we used 16 moisture soundings distributed evenly over the domain, a surface moisture observation from each station in the 40-km network, and the integrated slant water vapor observations.

Figure 2 shows a horizontal plot of specific humidity (g kg^{-1}) at the 750-m above ground level (AGL) for the test area of the western United States. Note that the area goes from central Montana in the north to southern New Mexico in the south, and from central Utah to central Kansas in the east–west direction. Fig. 2a is the nature run, and Fig. 2b is the field recovered from the 3DVAR analysis. Starting with the nature run, a number of features are evident. A strong gradient of water vapor, the ''dryline,'' is evident from the Texas Panhandle up through central Kansas. An area of higher moisture values, with a maximum of 12.6 g kg^{-1}, is located just to the east of the dryline on the Oklahoma–Kansas border. Comparing the nature run with the 3DVAR, it is seen that the dryline has been recovered in the right place, with a decrease in the horizontal gradient. This is what would be expected from a 40-km grid spacing, where the nature field is created at 10-km resolution. Notice that the 3DVAR analysis recovered a moisture value of 12.9 g kg^{-1} on the Oklahoma–Kansas border moisture maximum. A large portion of the southwestern part of the domain has rather low values of specific humidity. Compare the minimum of moisture of 0.592 g kg^{-1} near the Colorado–Wyoming–Nebraska triple point with the 3DVAR minimum of 0.505 g kg^{-1} slightly to the south. Similarly, compare the value of the maximum in western Colorado of 2.10 g kg^{-1} in the nature run with the 2.19 g kg^{-1} located slightly to the north in the 3DVAR analysis.

Across the northern portion of the nature run are a series of small-scale maxima of moisture due to precipitation, which had fallen earlier. For example, note the maximum of 14.3 g kg^{-1} near the Nebraska–South Dakota border, two maxima on either side of the Wyoming–South Dakota border, and the maxima near the Wyoming–Idaho–Utah triple point. These should be compared with the same maxima in the 3DVAR analysis. Again, it is seen that the gradients are somewhat smoothed and the values are typically within 10%–20% of the nature run. In summary, at the 750-m level, typically in the middle of the boundary layer, the moisture analysis is far superior to that which could be obtained from the current network of radiosondes. Furthermore, this type of analysis would be available hourly, in contrast to the radiosondes, which only go up twice a day.

Figure 3 shows a horizontal plot of specific humidity

Unauthenticated | Downloaded 04/01/23 09:52 AM UTC

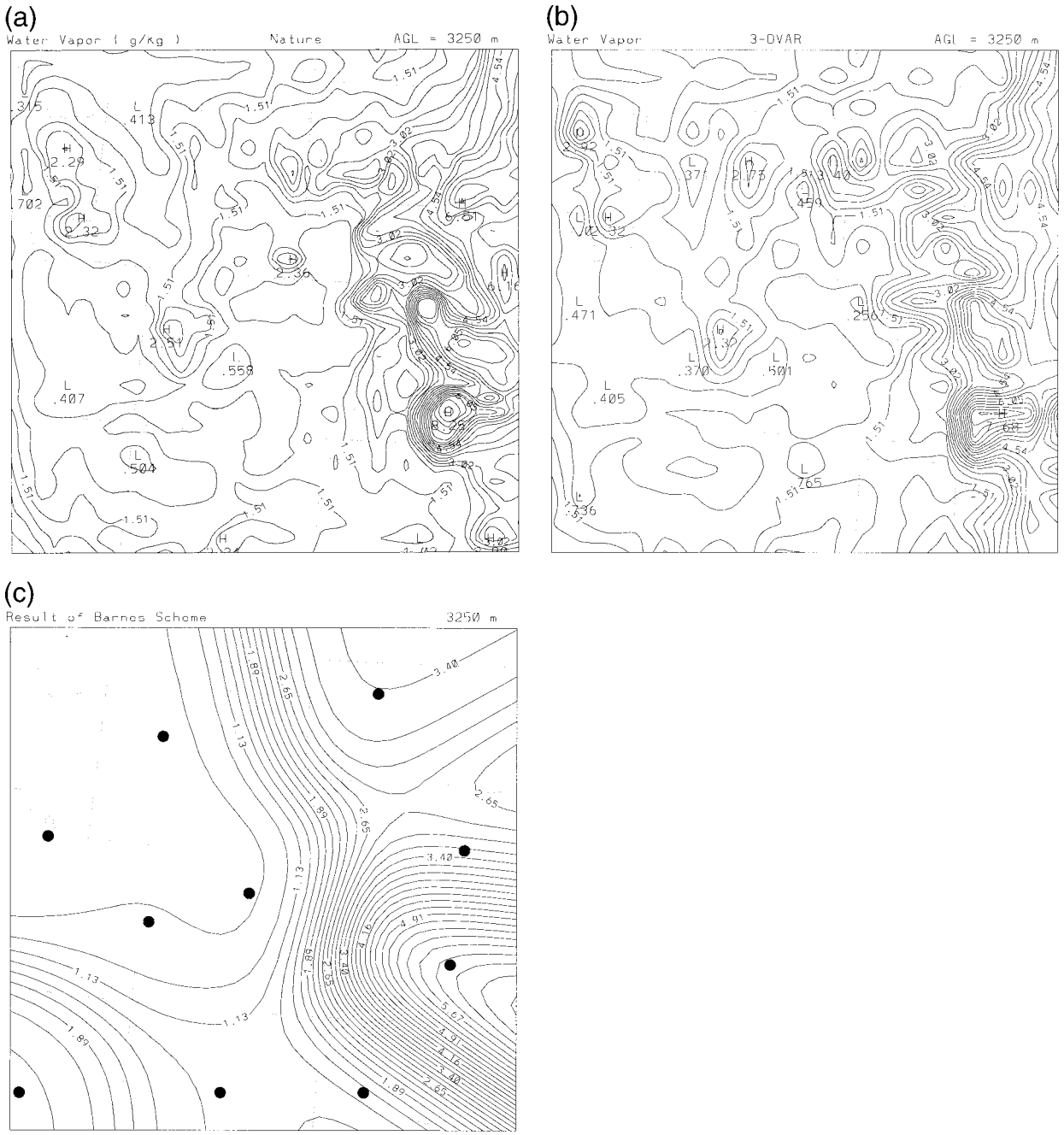

FIG. 3. Horizontal plots of specific humidity (g kg^{-1}) for (a) the nature, (b) 3DVAR, and (c) Barnes analysis at the 3250-m level. The nature run is from the Apr QNH case.

at 3250 m AGL for the nature run, 3DVAR, and a Barnes (1981) analysis. The Barnes analysis is presented to show the moisture diagnosis available from the current observing system. The black dots mark the location of radiosonde sites that were used in the analysis. A striking difference between the Barnes analysis (Fig. 3c) and the nature and 3DVAR analyses is its smoothness. The Barnes analysis only captures the synoptic-scale moisture variability. This is a reflection of the fact that the current upper-air observing system undersamples the moisture field (Emanuel et al. 1995). Again, similar to the discussion of the 750-m level, it can be seen from Figs. 3a and 3b that the 3DVAR captures the small-scale mesobeta moisture fields with reasonable accuracy.

Figure 4 shows plots of specific humidity at the 3250-m-level from the January MM5 case. The nature run, Fig. 4a, shows higher moisture values along the eastern

Unauthenticated | Downloaded 04/01/23 09:52 AM UTC

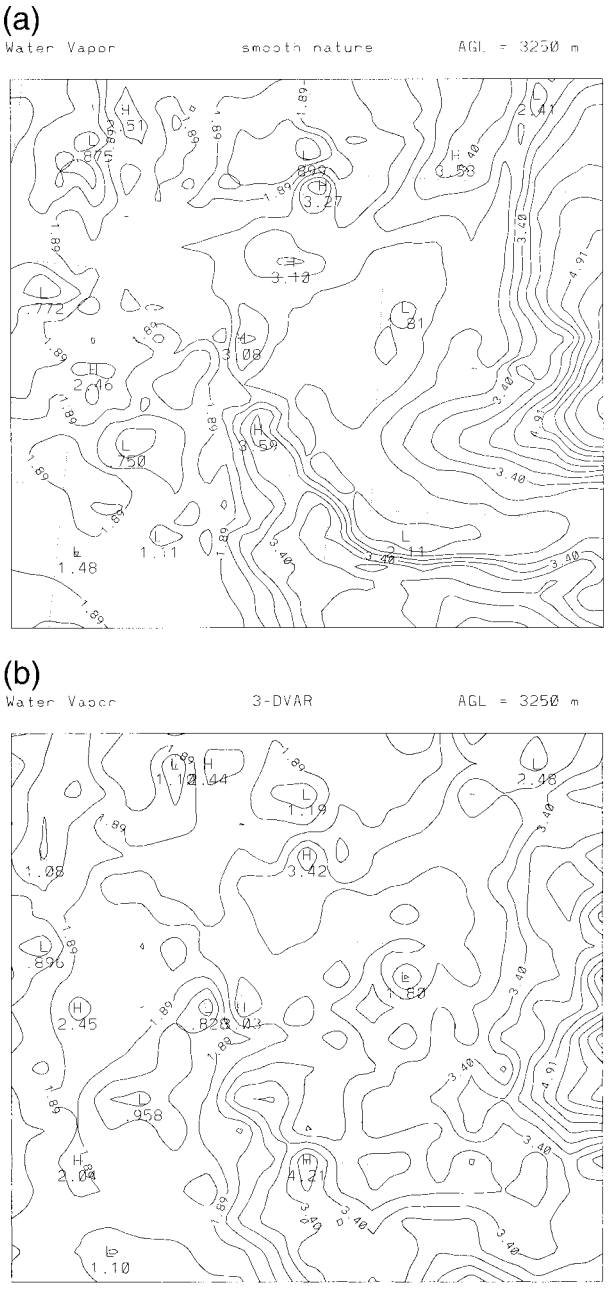

FIG. 4. Horizontal plots of specific humidity (g kg^{-1}) at the 3250-m level for (a) the nature, and (b) the 3DVAR case for the Jan MM5 case.

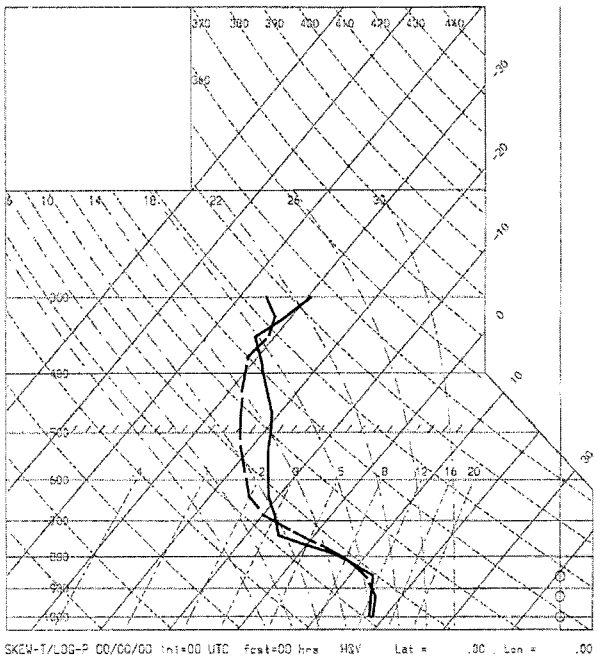

FIG. 5. Skew *T*–log*P* diagram comparing the moisture soundings. The solid line is from the nature run and the dashed line is from the 3DVAR analysis. This sounding, from the Apr QNH test, shows that the slant water vapor analysis is able to recover the strong gradient of moisture between 850 and 750 mb seen in the nature run.

border and a lobe of moisture from the Texas Panhandle into southern Colorado. These features are in the 3DVAR, Fig. 4b, but are not as well defined. The small features over the mountains have corresponding features in the 3DVAR analysis. In general, the 3DVAR does not do as well for drier parts of the atmosphere because it is minimizing on the rms of the field—an rms of 0.5 g kg^{-1} is a bigger percentage error when the field value is 1 g kg^{-1} than it is when the field is 10 g kg^{-1}.

A skew *T*–log*P* moisture sounding for the April QNH case is presented in Fig. 5. There are two curves: the solid curve from the nature run and the dashed curve from the 3DVAR. The location of the sounding, picked to be in a moist area, is marked with an asterisk in Fig. 2. The 3DVAR captures the moist layer from the surface to 850 mb and the transition from moist to dry between 850 and 750 mb. The 3DVAR is drier in the layer from 700–400 mb. The lower accuracy seen in the upper troposphere is discussed in the next section. This sounding is an excellent example of the rationale for using the slant water vapor observations. The strong vertical gradient of moisture between 850 and 750 mb is very important, and could never be gleaned from the use of vertically integrated water vapor measurements.

b. Quantitative comparison

The OSS approach allows comparison of different analysis techniques against the ''truth,'' that is, the nature field. In this study, the 3DVAR analysis derived from the hypothetical 40-km-spaced network of GPS slant water vapor, surface stations, and a few vertical soundings can be compared with the Barnes analysis that would be obtained from the existing radiosonde network. Note that the radiosonde locations are shown in Fig. 3c.

We calculated three quantities: the percent error (pce), the rms error, and the bias. These quantities are defined as

Unauthenticated | Downloaded 04/01/23 09:52 AM UTC

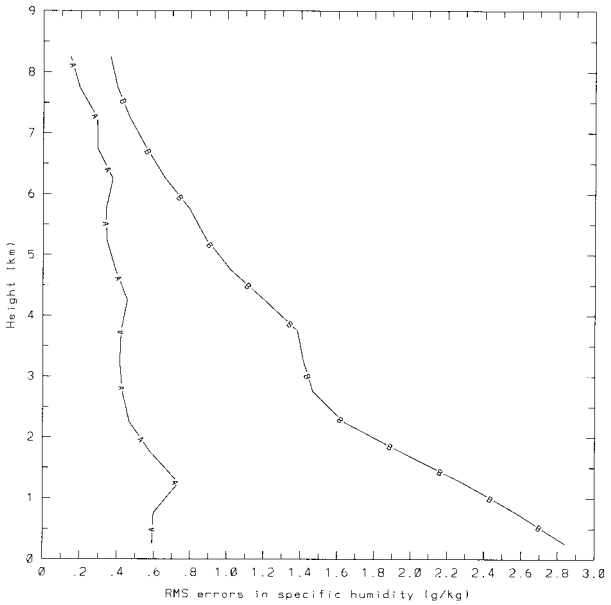

FIG. 6. A vertical plot of the rms error of specific humidity (g kg^{-1}) against the nature run from the QNH Apr case using the 3DVAR (A curve) and the Barnes scheme (B curve).

$$E_{\text{pce}} = \sqrt{\frac{\sum_{i=1,j=1,k=1}^{N_x,N_y,N_z} (q_{i,j,k}^{\text{Est}} - q_{i,j,k}^{\text{Tru}})^2}{\sum_{i=1,j=1,k=1}^{N_x,N_y,N_z} (q_{i,j,k}^{\text{Tru}})^2}},$$

$$E_{\text{rms}} = \sqrt{\frac{\sum_{i=1,j=1,k=1}^{N_x,N_y,N_z} (q_{i,j,k}^{\text{Est}} - q_{i,j,k}^{\text{Tru}})^2}{N_x N_y N_z}}, \quad \text{and}$$

$$E_{\text{bias}}(k) = \frac{\sum_{i=1,j=1}^{N_x,N_y} (q_{i,j,k}^{\text{Est}} - q_{i,j,k}^{\text{Tru}})^2}{\sum_{i=1,j=1}^{N_x,N_y} (q_{i,j,k}^{\text{Tru}})}.$$

Table 1 shows the rms error of the two simulations. In both cases, the rms error of the 3DVAR slant water vapor network is smaller by a factor of 2 than the Barnes analysis of the radiosonde network. This substantial reduction should make a difference in model predictions and analysis of fields such as the lifted index. Similarly, the pce, shown in Table 2, indicates that the 3DVAR approach is better by a factor of two in both simulations.

We also studied the rms and bias as a function of height above ground. Figure 6 shows the rms for the April case. It can be seen that the rms of the Barnes analysis of radiosondes starts out quite large, about 2.8 g kg^{-1} near the surface, and decreases with height up to 8 km. The general decrease is because the lower atmosphere is far more moist, with a typical scale height for moisture of between 2 and 3 km. The 3DVAR has an error of about 0.6 g kg^{-1} near the surface, with similar values all the way to 8 km. Note that the goal of the 3DVAR algorithm is to equalize rms errors over the whole domain. It is clear from Fig. 6 that it was quite successful in this case, converging to a similar error regardless of altitude. As a result, the 3DVAR slant water vapor network analysis is far superior in the lower levels, but actually inferior at levels above 6.5 km. This suggests that if the moisture of the upper troposphere were more important than that of the lower troposphere, the 3DVAR could be weighted to do a better job at higher altitudes. In fact, the low- and midtropospheric moisture analysis is more important for weather prediction simply because the amount is so much larger in the lower levels.

TABLE 1. The rms errors of the specific humidity (g kg^{-1}) for the 3DVAR analysis from GPS network on the top line, and for the Barnes analysis on the bottom line.

Network	QNH	MM5
GPS network	3.4×10^{-3}	2.4×10^{-3}
Barnes raob	7.7×10^{-3}	7.6×10^{-3}

TABLE 2. Percent errors for the 3DVAR from the GPS network on the top line and from the Barnes analysis of the radiosonde network on the bottom line.

Network	QNH	MM5
GPS network	20%	14%
Barnes	47%	33%

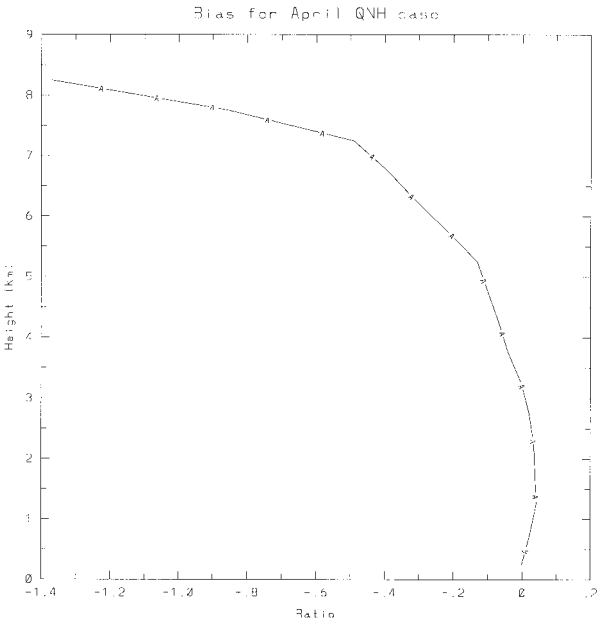

FIG. 7. Bias for the Apr QNH case. Bias is defined as the departure of the 3DVAR field average from the nature run. Positive values indicate a dry bias, and negative values indicate a moist bias. Bias and accuracy are poorer above 6 km where moisture amounts approach the full-domain average 3DVAR error of 0.5 g kg^{-1}.

Unauthenticated | Downloaded 04/01/23 09:52 AM UTC

TABLE 3. Specific humidity (g kg^{-1}) rms errors at 850 mb and 500 mb for radiosondes, the 3DVAR from the GPS network, the RUC model first guess, and the Barnes analysis. The GPS simulation provides moisture estimates significantly better than model guess fields, but inferior to radiosondes.

Network	850 mb	500 mb
Radiosondes	0.47	0.30
GPS network	0.70	0.53
RUC guess	1.95	0.74
Barnes	2.50	0.80

The 3DVAR slant water vapor bias for the April case is shown in Fig. 7. The bias is near zero (unbiased) up to about 6 km, and negative (a moist bias) above that level. Evidently the 3DVAR is insensitive to the actual very dry air in the upper levels as it attempts to reach a minimum difference over the entire domain.

The estimate of rms errors as a function of height in Fig. 6 allows comparison with error estimates from other sources. The National Centers for Environmental Prediction (NCEP) recently published estimated errors for radiosondes (Zapotocny et al. 2000), and Smith et al. (2001) have estimated moisture errors from the RUC model. The rms errors at two levels, 850 mb and 500 mb, were interpolated from Fig. 6 and compared with the NCEP and RUC errors. The results, shown in Table 3, indicate that the radiosonde is most accurate at both levels, with the simulated GPS network showing a significantly reduced error compared to the RUC first-guess field and the Barnes analysis. Although inferences from a single case should be limited, it is encouraging to see the GPS network-derived errors much closer to the radiosonde at 850 mb than the model guess.

An important distinction must be made between the hypothetical analysis obtained from the radiosonde network versus the GPS slant water vapor network. Now, and in the foreseeable future, the radiosondes are only released twice a day in the United States. The hypothetical slant water vapor network would deliver a three-dimensional analysis every hour. Thus, the comparisons shown in this section would be significantly stronger in favor of the slant water vapor network since a typical analysis would be ''off time,'' that is, other than the radiosonde time. Continuous hourly moisture analysis would be helpful in severe convective weather prediction and other short-range forecast problems where rapid change is important (Emanuel et al. 1995).

6. Conclusions

A hypothetical network of ground-based GPS receivers, surface hygrometers, and lower density of moisture sounding devices has been described. An OSS used nature atmospheres from mesoscale models to assess the ability of the proposed observational network to return accurate three-dimensional moisture fields. The results of the OSS suggest that such a network would significantly increase the accuracy and specificity of moisture diagnosis.

The validity of water vapor analysis is dependent on a number of assumptions, such as the measurement of slant water vapor at angles below 6°. If measurements can be obtained with reasonable accuracy to a degree above the horizon, the network would provide moisture fields down to the surface. Correlation between small-scale mass and moisture fields could also cause difficulties. Finally, the measurement of the signal phase delay is affected by other entities, such as heavy rain (Solheim et al. 1999), which could be corrected using weather radars. A study of this type is suggestive, but not definitive concerning the role that such a network could play in operational weather prediction, particularly since history has shown that such studies err on the optimistic side. The best way to determine the value of such a system would be to field a demonstration network large enough to develop and test the concept over a period of at least a couple of years.

It is important to mention the value of accurate hourly diagnosis of the three-dimensional moisture field for areas other than meteorology. Highly accurate GPS location is partially limited by the unknown distribution of moisture and mass in the atmosphere. There are numerous potential applications of GPS that require great accuracy, such as landing an airplane. A national analysis of water vapor and a ''delay function'' could be made available through the Internet or some other distribution and used in GPS calculations to make them more accurate. This would be a very important additional benefit from the proposed high-resolution network of ground-based GPS sensors.

This study demonstrates that it may be feasible to determine the three-dimensional water vapor field at high temporal (every hour) and spatial (mesobeta) resolutions with much higher accuracy than currently available. We believe that such a network, used in conjunction with a high-resolution mesoscale weather prediction model, might deliver a significant improvement in prediction of precipitation and severe weather.

Acknowledgments. We would like to thank Chris Davis and Jin Luen Lee for providing the model data used in this study. We would also like to thank Tom Schlatter, Chris Rocken, Rick Anthes, Bill Kuo, and Seth Gutman for helpful discussions of this concept.

REFERENCE

Alber, C., R. Ware, C. Rocken, and J. Braun, 2000: Obtaining single path phase delays from GPS double differences. *Geophys. Res. Lett.*, **27,** 2661–2664.

Barnes, S. L., 1981: *SESAME 1979 Data User's Guide.* Project SESAME, U.S. Department of Commerce, NOAA/ERL, 236 pp.

Bevis, M., S. Businger, T. A. Herring, C. Rocken, R. A. Anthes, and R. H. Ware, 1992: GPS meteorology: Remote sensing of atmospheric water vapor using the Global Positioning System. *J. Geophys. Res.*, **97,** 15 787–15 801.

Unauthenticated | Downloaded 04/01/23 09:52 AM UTC

——, ——, S. Chiswell, T. Herring, R. Anthes, C. Rocken, and R. Ware, 1994: GPS meteorology: Mapping zenith wet delays onto precipitable water. *J. Appl. Meteor.,* **33,** 379–386.

Braun, J., C. Rocken, and R. Ware, 2001: Validation of single slant water vapor measurements with GPS. *Radio Sci.,* **36,** 459–472.

Byrd, R., P. Lu, J. Nocedal, and C. Zhu: 1995: A limited memory algorithm for bound constrained optimization. *SIAM J. Sci. Comput.*, **16,** 1190–1208.

Chen, G., and T. Herring, 1997: Effects of atmospheric azimuthal asymmetry on the analysis of space geodetic data. *J. Geophys. Res.*, **102** (B9), 20 489–20 502.

Davis, J., G. Elgered, A. Niell, and C. Kuehn, 1993: Ground-based measurement of gradients in the ''wet'' radio refractivity of air. *Radio Sci.,* **28,** 1003–1018.

Dudhia, J., 1993: A nonhydrostatic version of the Penn State–NCAR Mesoscale Model: Validation tests and simulation of an Atlantic cyclone and cloud front. *Mon. Wea. Rev.*, **121,** 1493–1513.

Elosegui, P., J. Davis, L. Gradinarsky, G. Elgered, J. Johansson, D. Tahmoush, and A. Rius, 1999: Sensing atmospheric structure using small-scale space geodetic networks. *Geophys. Res. Lett.,* **26,** 2445–2448.

Emanuel, K., and Coauthors, 1995: Report of the First Prospectus Development Team of the U.S. Weather Research Program to NOAA and the NSF. *Bull. Amer. Meteor. Soc.*, **76,** 1194–1208.

Fang, P., M. Bevis, Y. Bock, S. Gutman, and D. Wolfe, 1998: GPS meteorology: Reducing systematic errors in geodetic estimates for zenith delay. *Geophys. Res. Lett.*, **25,** 3583–3596.

Güeldner, J., and D. Spänkuch, 2001: Remote sensing of the thermodynamic state of the atmospheric boundary layer by ground-based microwave radiometry. *J. Atmos. Oceanic Technol.,* **18,** 925–933.

Guo, Y. R., Y. H. Kuo, J. Dudhia, D. B. Parsons, and C. Rocken, 2000: Four-dimensional variational data assimilation of heterogeneous mesoscale observations for a strong convective case. *Mon. Wea. Rev.,* **128,** 619–643.

Kaplan, E., 1996: *Understanding GPS Principles and Applications.* Artech House, 522 pp.

Kuo, Y. H., Y. R. Guo, and E. R. Westwater, 1993: Assimilation of precipitable water measurements into a mesoscale model. *Mon. Wea. Rev.,* **121,** 1215–1238.

——, X. Zou, and Y. R. Guo, 1996: Variational assimilation of precipitable water using a nonhydrostatic mesoscale adjoint model. Part I: Moisture retrieval and sensitivity experiements. *Mon. Wea. Rev.,* **124,** 122–147.

Liu, D., and J. Nocedal, 1989: On the limited memory BFGS method for large-scale optimization. *Math. Program.,* **B-45,** 503–528.

Lowry, A., S. Sokolovskiy, C. Rocken, and K. Anderson, 2001: Vertical profiling of atmospheric refractivity from ground-based GPS observations. *Radio Sci.,* in press.

MacDonald, A., and Y. Xie, 2000: On the use of slant observations from GPS to diagnose three-dimensional water vapor using 3DVAR. Preprints, *Fourth Symp. on Integrated Observing Systems,* Long Beach, CA, Amer. Meteor. Soc., 62–73.

——, J. Lee, and S. Sun, 2000: QNH: Design and test of a quasi-nonhydrostatic model for mesoscale weather prediction. *Mon. Wea. Rev.,* **128,** 1016–1036.

Niell, A., 1996: Global mapping functions for the atmosphere delay at radio wavelengths. *J. Geophys. Res.,* **101,** 3227–3246.

Palmen, E., and C. W. Newton, 1969: *Atmospheric Circulation Systems.* Academic Press, 603 pp.

Rocken, C., R. Ware, T. Van Hove, F. Solheim, C. Alber, J. Johnson, M. Bevis, and S. Businger, 1993: Sensing atmospheric water vapor with the Global Positioning System. *Geophys. Res. Lett.*, **20,** 2631–2634.

——, T. Van Hove, and R. Ware, 1997: Near real-time sensing of atmospheric water vapor. *Geophys. Res. Lett.,* **24,** 3221–3224.

——, S. Sokolovskiy, J. Johnson, and D. Hunt, 2001: Improved mapping of tropospheric delays. *J. Atmos. Oceanic Technol.,* **18,** 1205–1213.

Segall, P., and J. Davis, 1997: GPS applications for geodynamics and earthquake studies. *Annu. Rev. Earth Planet. Sci.,* **25,** 301–336.

Smith, T. L., S. Benjamin, B. Schwartz, and S. Gutman, 2001: Using GPS-IPW in a 4-D data assimilation system. *Earth, Planets Space,* in press.

Sokolovskiy, S., C. Rocken, and A. Lowry, 2001: The use of GPS for estimation of bending angles of radio waves at low elevations. *Radio Sci.,* **36,** 473–482.

Solheim, F., J. Godwin, E. Westwater, Y. Han, S. Keihm, K. Marsh, and R. Ware, 1998: Radiometric profiling of temperature, water vapor, and liquid water using various inversion methods. *Radio Sci.,* **33,** 393–404.

——, J. Vivekanandan, R. Ware, and C. Rocken, 1999: Propagation delays induced in GPS signals by dry air, water vapor, hydrometeors, and other particulates. *J. Geophys. Res.,* **104** (D8), 9663–9670.

Ware, R., C. Alber, C. Rocken, F. Solheim, 1997: Sensing integrated water vapor along GPS ray paths. *Geophys. Res. Lett.,* **24,** 417–420.

——, D. Fulker, S. Stein, D. Anderson, S. Avery, R. Clark, K. Droegemeier, J. Kuettner, J. Minster, and S. Sorooshian, 2000: SuomiNet: A real-time national GPS network for atmospheric research and education. *Bull. Amer. Meteor. Soc.,* **81,** 677–691.

Wolfe, D. E., and S. I. Gutman, 2000: Developing an operational, surface-based, GPS, water vapor observing system for NOAA: Network design and results. *J. Atmos. Oceanic Technol.,* **17,** 426–440.

Zapotocny, T. H., and Coauthors, 2000: A case study of the sensitivity of the Eta data assimilation system. *Wea. Forecasting,* **15,** 603–621.

Unauthenticated | Downloaded 04/01/23 09:52 AM UTC